J. Fluid Mech. (1992), *vol.* 234, *pp.* 71–96
Printed in Great Britain

The response and symmetry properties of a cylinder wake subjected to localized surface excitation

By DAVID R. WILLIAMS, HUSSEIN MANSY AND CLIFF AMATO

Mechanical and Aerospace Engineering Department, Illinois Institute of Technology, Chicago, IL 60616, USA

(Received 30 January 1991 and in revised form 6 June 1991)

Symmetric and antisymmetric periodic disturbances introduced directly into the boundary layer on a circular cylinder at low Reynolds number are shown by experiment to be capable of modifying the vortex formation process and changing the vortex shedding frequency. Spectral measurements have shown that the antisymmetric vortex shedding mode is strongly coupled to the symmetric first harmonic mode. When symmetric excitation is applied, three different shapes of the mean velocity profiles can be identified as the forcing amplitude is increased. At low forcing amplitudes nonlinear interaction between the forcing field and the natural wake oscillator produces sum and difference modes. Symmetric forcing with intermediate-amplitude disturbances suppresses the natural shedding frequency, and the dominant vortex shedding energy appears as a sinuous mode at half the excitation frequency. At high symmetric forcing amplitudes a threshold is reached, above which the large-scale vortices do not form. The symmetries of the combination modes follow two simple rules based on the symmetries of the interacting modes. The symmetry rules provide an explanation for the fundamental difference in wake structure that occurs between symmetric forcing and antisymmetric forcing.

1. Introduction

Substantial progress has been made over the last five years toward understanding the instability mechanism that determines the vortex shedding frequency in the wake of bluff bodies. Koch (1985), Monkewitz & Nguyen (1987), Triantafyllou, Triantafyllou & Chryssostomidis (1986), and Hanneman & Oertel (1989) have used the concepts of linear stability theory to prove the existence of local absolute instability in the near-wake region at supercritical Reynolds numbers. Chomaz, Huerre & Redekopp (1988) using the Ginzburg–Landau model have shown that absolute instability is a necessary but not a sufficient condition for self-sustained oscillations. A sufficiently large region of absolute instability is required for the global instability that leads to the self-sustained oscillations. Monkewitz (1988) has shown that the stability characteristics of wakes follow the prediction of Chomaz *et al.* Experiments by Provensal, Mathis & Boyer (1987) and Sreenivasan, Strykowski & Olinger (1987) have demonstrated that vortex shedding near the critical Reynolds number is the result of a temporal global instability. Thus, the *initiation* of the wake oscillations is reasonably well understood.

As the instability grows to finite amplitudes, nonlinear effects become important. The first harmonic of the vortex shedding frequency appears in the wake, and a

saturation amplitude or limit-cycle state is reached. At this stage the near wake produces fully formed Kármán vortices. Morkovin (1964) and Gerrard (1978) have given descriptions of a large variety of wake phenomena that occur as the Reynolds number is changed. Hanneman & Oertel (1989) have used numerical simulation to study the evolution from the linear stages to the nonlinear self-excited stage of vortex development in the wake of a bluff body.

The initial disturbances for the self-sustained oscillations in the nonlinear saturated state are provided by the vorticity dynamics in the wake. The self-excitation cycle (resonance) consists of the modulation of the boundary layer by initial disturbances on the body, followed by spatial amplification of the disturbances in the separated shear layers, leading to the fully formed vortices which produce the feedback signal to the body. The feedback signal has been observed in the experiments by Nishioka & Sato (1978) and Unal & Rockwell (1987*a*). Their measurements have shown the velocity fluctuation level in the vicinity of the body surface to be relatively large, i.e. about 3% of the free-stream velocity at Reynolds number of 150. If a splitter plate is used to suppress the vortex formation, then the initial disturbances on the body are decreased to background levels (Unal & Rockwell 1987*b*). It is not clear, however, if the upstream influence occurs by the induced velocity field of the vortices (Biot–Savart induction) or by upstream-travelling vorticity waves resulting from the initial global instability. Rockwell (1990) refers to the latter mechanism as type-I global instability and the former as type-II global instability.

In either case, the essential elements of the unforced near-wake resonance can be summarized as: (i) upstream influence providing initial spatio-temporal disturbances to the shear layers on the body, i.e. a feedback signal; (ii) cross-flow communication between the two separated shear layers; (iii) spatial amplification of the disturbances in the separated shear layers to a saturation level which provides the feedback signal.

Since the wake structure is determined by the resonance mechanism, and the steady and unsteady forces acting on the body are determined to a large extent by the wake structure, it follows that the forces can be controlled by modifying the mechanism of the self-excitation process. One example is the splitter plate, which breaks the resonance in the wake by preventing cross-flow communication and changing the boundary condition on the wake centreline (see Unal & Rockwell 1987*b*). As a result the Kármán vortex street does not form, and there is a significant reduction in the drag on the body.

Other examples of wake control include base bleed (Bearman 1967; Wood 1964, 1967), oscillating the cylinder (Koopman 1967; Berger 1967; Wehrmann 1967; Griffin & Ramberg 1976; Bearman 1984; Olinger & Sreenivasan 1988) and excitation with sound (Blevins 1985; Detemple-Laake & Eckelmann 1989; Ffowcs Williams & Zhao 1988). These are global types of forcing, since a large region of the flow is disturbed. In these experiments a change in the large-scale wake structure has been observed, but the reasons for the change are not clear. It is difficult to determine exactly how the forcing field interacts with the near-wake resonance mechanism, because the forcing affects a large area of the flow. With sound wave excitation, for example, there is modulation of the attached boundary layer, the separating shear layers, as well as the wake. By introducing disturbances at specific, well-defined locations, one can obtain a better understanding of the wake oscillation mechanism.

The purpose of the present set of experiments is to investigate the possibility of using *local* forcing to interact directly with the feedback signal on the surface of the body. In particular, we wish to determine if nonlinear interaction can occur between the localized forcing field and the feedback signal from the wake. Assuming that such

an interaction does take place, then the effect of the local forcing on the large-scale vortex formation process will be examined. New insight into the physics of self-sustained oscillations can be gained by comparing the wake in its forced state with the unforced free oscillations. Our experiment investigates these issues by using the unsteady bleed technique to introduce disturbances into the boundary layer at $\pm 45°$ from the forward stagnation line.

The following section describes the unsteady bleed forcing technique, and the experimental methods used to acquire and process the data. The results presented in §3 describe the effects of symmetric and antisymmetric excitation. The interpretation of the results is discussed in §4. Section 5 presents the conclusions.

2. Experimental method

The experiments were conducted on a small recirculating water channel with a test section 20.3 cm wide, 30.5 cm high and 244 cm in length. The typical operating speed, U_0, was 4.5 cm/s, which gave a Reynolds number based on the cylinder diameter of 470. The free-stream turbulence level was measured with a hot-film probe to be 0.22% of the free-stream velocity. The mean flow in the central 10 cm width of the channel was constant to within 0.5% of U_0.

The water channel was covered to reduce surface waves, and a slot was milled in the top through which the cylinder was positioned. Rather than move the optics of the laser anemometer, the cylinder was moved in the water channel to obtain measurements at different streamwise locations. The origin of the coordinate system was defined as the centre of the cylinder. The x-axis and u-velocity component were in the streamwise direction, the y-axis was perpendicular to the flow direction and the cylinder axis. The z-axis was coincident with the axis of the cylinder.

The cylinder was constructed from a hollow piece of Lexan plastic with an outer diameter $D = 0.954$ cm and an inner diameter of 0.635 cm. The outer diameter was uniform to 0.28% of D. Circular end plates were placed 18 cm apart on the cylinder to promote parallel vortex shedding. The aspect ratio L/D for the cylinder between the end plates was 18.9. Since the blockage in the channel was only 4.7%, no correction was applied to the data.

Two rows of small holes ($d_j = 0.074$ cm) were drilled along the axis of the cylinder at $\theta = \pm 45°$, where θ is the angle measured from the forward stagnation line as shown in figure 1. There were 131 holes per row. A Plexiglas dividing wall was cemented inside the cylinder between the two rows of holes to form two separate chambers. The internal chambers of the cylinder were connected with Tygon tubing to a dual piston–cylinder forcing mechanism shown schematically in figure 1. With this system the two rows of holes could be forced either in-phase (symmetric forcing) or 180° out of phase (antisymmetric forcing). The diameter and spacing of the holes were small enough that the effective disturbance was two-dimensional over the length of the cylinder.

The forcing system was completely closed except for the bleed holes on the surface of the cylinder. During the outflow phase a small amount of water was ejected from the holes, and the same volume of water was drawn back into the cylinder during the inflow phase. By continuity, there is zero net mass addition to the flow on average over the forcing cycle. However, owing to the nonlinear streaming effect there is momentum addition to the flow. The streaming effect can be significant enough at high forcing levels to change the base flow state, as shown by Williams & Amato (1989).

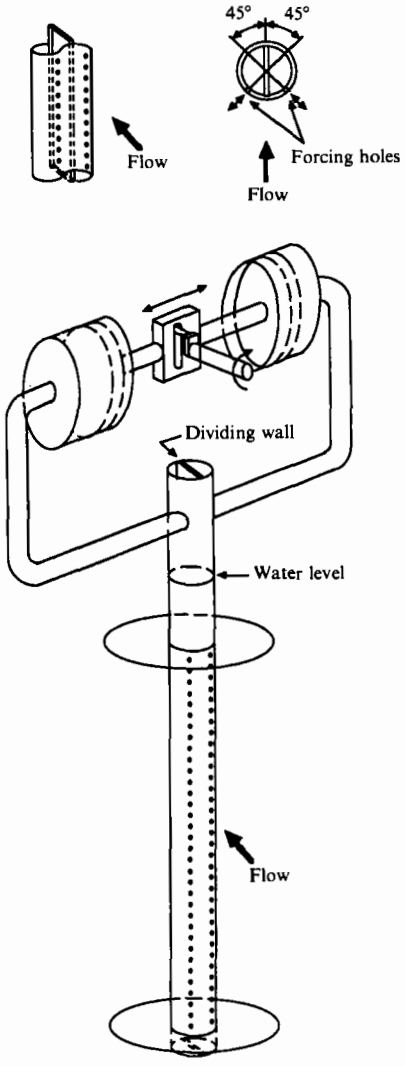

FIGURE 1. Schematic of the cylinder and unsteady bleed system.

The measure of excitation amplitude used in this experiment is the bleed coefficient, C_b, which is defined as $(u_j'^2 d_j)/(U_0^2 D)$, where u_j' is the r.m.s. velocity of the flow at the exit of the unsteady bleed jet. The bleed coefficient represents the momentum induced by the unsteady bleed jets relative to the momentum in the undisturbed free stream. The value of u_j' was determined from the forcing frequency, f_e, and the amplitude of the displacement of the air–water interface in the tubing leading to the cylinder model.

The hydrogen bubble technique was used for flow visualization. The bubbles were generated with a 0.025 mm diameter platinum wire, which was soldered to a copper frame. A 450 mA current at 30 V was used to ionize the water and produce the hydrogen bubbles.

Quantitative measurements of the streamwise velocity component, u, were obtained with the scanning laser anemometer (SLA) shown schematically in figure 2.

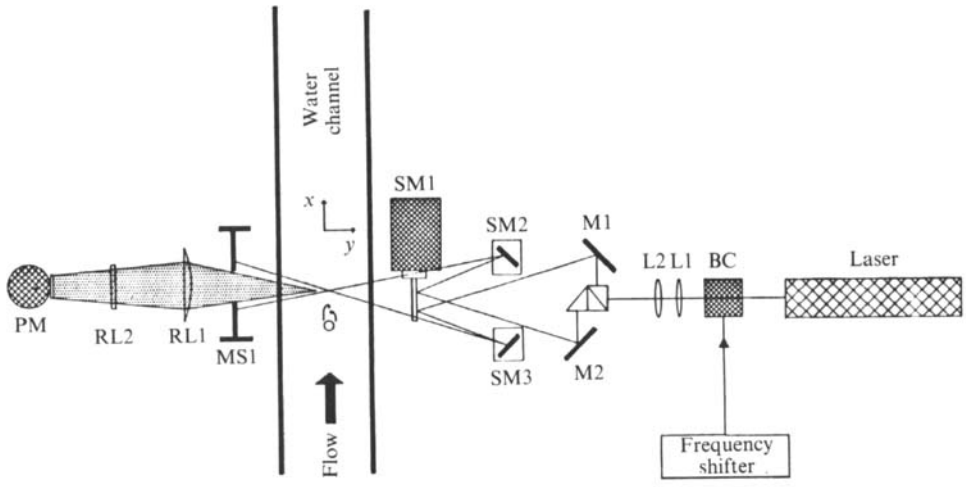

FIGURE 2. Schematic of the scanning laser anemometer system. BC, bragg cell; L1, L2, beam focusing lenses; BS, beam splitter and prism; M1, M2, mirrors; SM1, vertical optical scanner; SM2, SM3, horizontal optical scanner; MS1, mask; RL1, RL2, cylindrical lenses; PM, photomultiplier tube.

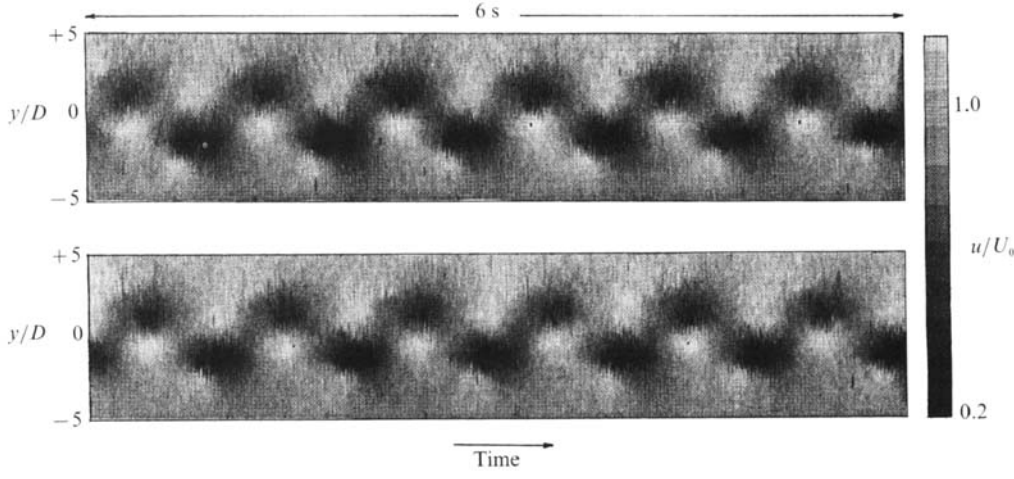

FIGURE 3. Twelve seconds of linearly interpolated SlA data prior to spectral processing obtained at $x/D = 4.0$ are shown. The speed of the flow is indicated by the grey level.

Details of the system may be found in Williams & Economou (1987). The SLA system is a typical forward-scatter laser anemometer, whose beam crossing location is controlled by electro-mechanical scanners. The position of the measurement volume was determined with the feedback signal from the scanners to within 0.5 mm over a 10 cm scan length. The scan rates were varied from 10 to 40 scans/s depending on the type of measurement. Frequency shifting at 50 kHz was used. The flow was seeded with 2.0 μm polystyrene spheres. Data rates on the counter processor were as high as 6000 valid measurements per second, but were varied depending on the type of measurement being made.

With the SLA one obtains quasi-instantaneous velocity profiles as a function of time. An interpolation routine was used to convert the randomly spaced raw data

into 128 evenly spaced bins along each scan across the flow. One of the interpolated data sets is shown in figure 3, where the grey level represents the magnitude of the velocity. Each bin represents a different y-location. Any desired y-location (or a separate external signal) can be used as a reference signal for the cross-spectra calculations. The autospectra and cross-spectra have been computed for each y-location with a frequency resolution of 0.019 Hz. Typically 15 ensemble averages of 512 points per ensemble-bin have been used to compute the spectral estimates. The low number of ensembles is due to storage limitations on the data acquisition computer. The end result of the post processing is a data set with high spatio-temporal resolution of the mean, r.m.s., amplitude, phase and coherence distributions across the wake.

3. Results

A preliminary set of experiments was conducted with the unsteady bleed holes located at $\pm 135°$ from the forward stagnation line. The idea was to excite the shear layers shortly after separation with symmetric disturbances. Surprisingly, there was almost no detectable influence on the wake structure until very large forcing amplitudes were reached. Distortion of the mean flow by the streaming effect was clearly seen in the flow visualization at high forcing levels. It was concluded that the separated shear layers were not receptive to this type of excitation, and no further studies were conducted.

Introducing disturbances into the boundary layer before separation had a much larger effect on the wake development. In the next two sections the effect of forcing symmetrically (rows of jets in phase) at $\theta = \pm 45°$ and antisymmetrically (rows of jets 180° out of phase) are discussed.

3.1. *Symmetric forcing – time-averaged flow behaviour*

The flow visualization photographs in figure 4 show the wake in four different states: (*a*) the natural wake ($C_b = 0$), (*b*) the wake at a low-amplitude excitation ($C_b = 0.026$), (*c*) intermediate excitation ($C_b = 0.095$), and (*d*) high excitation amplitude ($C_b = 0.22$). All cases are at a fixed excitation frequency $f_e = 1.8f_0$, where f_0 is the natural Kármán shedding frequency. A dramatic change in the wake structure takes place as the forcing amplitude is increased. At low amplitudes the centres of the vortices in figure 4(*b*) move closer to the wake centreline, but the structure is essentially the same as the natural case. In figure 4(*c*) the increase in forcing amplitude to an intermediate level causes a rearrangement of the vortices. The vortex formation occurs much closer to the cylinder body, and the wake can be seen to spread at a much faster rate than the undisturbed natural wake. Comparing figure 4(*c*) with figure 4(*a*), one observes that the centres of the vortices cross the centreline of the wake, in contrast to the unforced case, where the vorticity shed from one side of the body remains on the same side. Similar patterns in the vorticity field were observed by Detemple-Laake & Eckelmann (1989) (their 'seahorse' pattern) and Williamson & Roshko (1988).

There is clearly a sinuous structure to the pattern of vortices seen in figure 4(*a–c*), however, when the forcing amplitude is increased above the threshold level, C_b^*, then the staggered vortex pattern is replaced by a parallel shedding arrangement as shown in figure 4(*d*). We refer to this as the 'over-forced' state. There is a large region of quiescent fluid extending about 5–6 diameters behind the body, and the spreading rate of the wake is dramatically reduced. Farther downstream at approximately

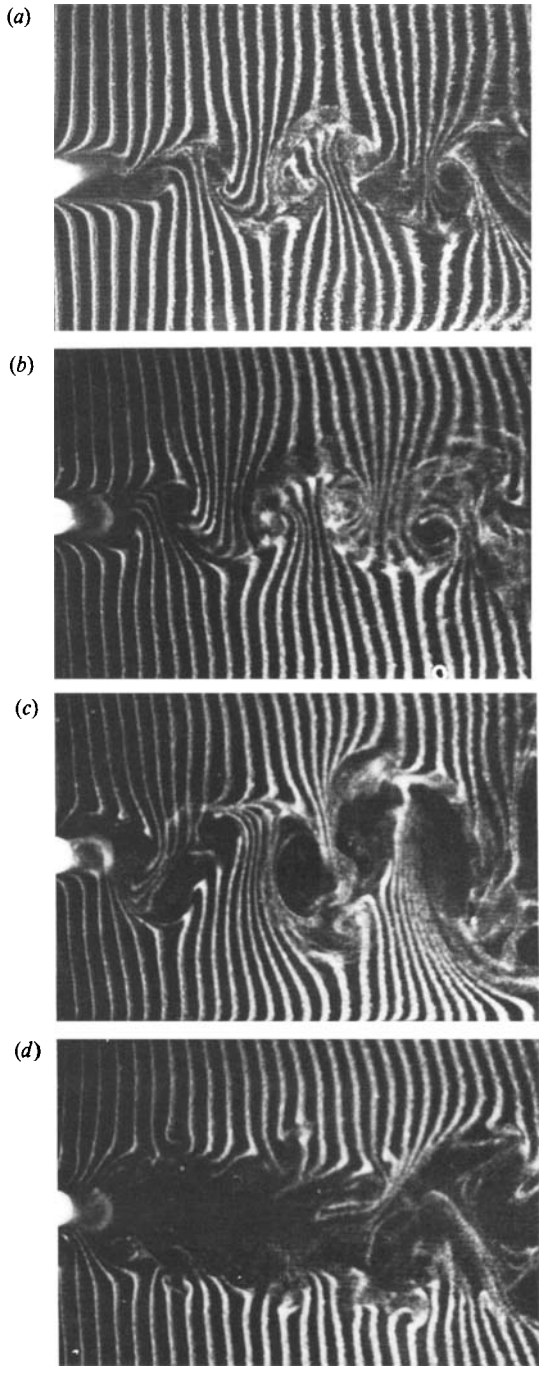

FIGURE 4. Hydrogen bubble flow visualization showing the natural wake and symmetric forcing case, $f_e/f_0 = 1.8$: (*a*) natural wake; (*b*) low-amplitude forcing, $C_b = 0.026$; (*c*) intermediate amplitude, $C_b = 0.095$; (*d*) high amplitude, $C_b = 0.22$.

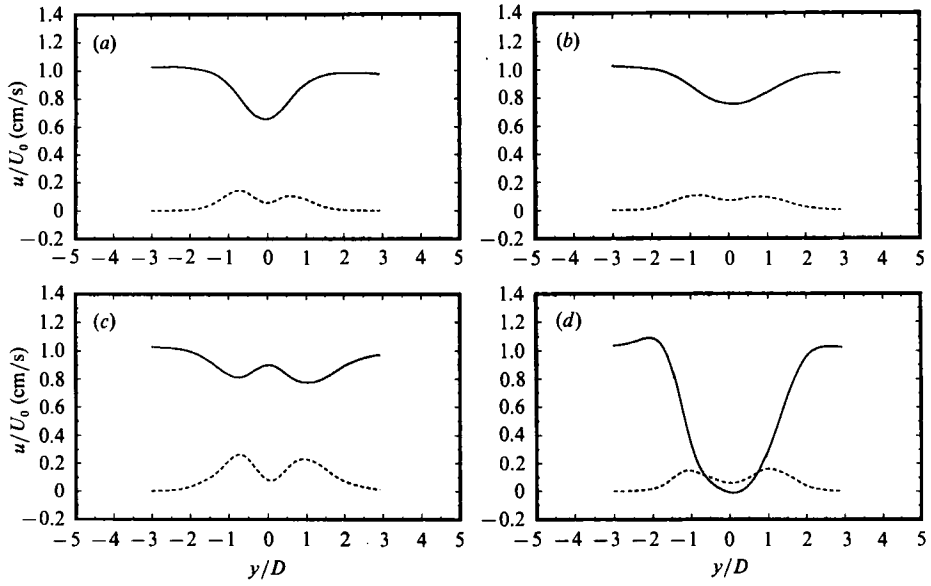

FIGURE 5. Mean and r.m.s. velocity profiles at $x/D = 4.0$ corresponding to the flow visualization cases shown in figure 4: (*a*) natural wake; (*b*) low-amplitude symmetric forcing, $C_b = 0.026$; (*c*) $C_b = 0.095$; (*d*) $C_b = 0.22$. The solid line is the mean profile and the dashed line is the r.m.s. profile.

$x/D = 6$, the wake develops a new sinuous mode of oscillation that appears to be somewhat weaker than the oscillations seen in figure 4(*a–c*).

The mean velocity profile $U(y)$ and root-mean-square (r.m.s.) velocity fluctuation distribution, $u'(y)$, at $x/D = 4$ are plotted in figure 5(*a–d*) corresponding to the previous flow visualization. With low-amplitude forcing the centreline velocity defect, $(U_0 - U_{c1})/U_0$, in the mean wake decreases from 0.37 to 0.25 as shown in figure 5(*b*). We refer to the mean profiles in figure 5(*a*, *b*) having a V-shape. The peak in the u' r.m.s. amplitude decreases from $0.15U_0$ in the natural wake to $0.10U_0$, which reflects a decrease in vortex strength. Although it has not been shown, the mean velocity defect and u' r.m.s. levels increase when very low forcing amplitudes are used. The low-level forcing produces stronger and more coherent vortices in the near-wake region. However, this phenomenon is frequency dependent, and has not yet been thoroughly investigated.

When the forcing amplitude is increased to $C_b = 0.095$, the mean velocity profile develops into a W-shape as shown in figure 5(*c*). The peak in the u' r.m.s. amplitude increases to about $0.25U_0$. The W-shaped mean velocity profilers are found at this particular forcing frequency, when forcing amplitudes are between $0.05 < C_b < 0.12$.

A simple explanation for the local maximum in the mean velocity profile at $y = 0$ can be found by examination of hydrogen bubble photographs. As mentioned earlier, when the Kármán vortex street forms in the unforced case, the vortices remain on the same side of the wake in which they are shed from the body. The induced velocity at $y = 0$ from this arrangement of vortices is in the upstream direction, which contributes to the centreline velocity defect and produces a V-shaped profile. However, when the centres of the vortices cross the wake centreline, the induced velocity is in the downstream direction. For example, vorticity shed from the right side of the body ends up on the left side of the wake. Consequently, the induced velocity from a fully formed vortex at $y = 0$ is in the downstream direction, which produces the local maximum of the W-shaped profile.

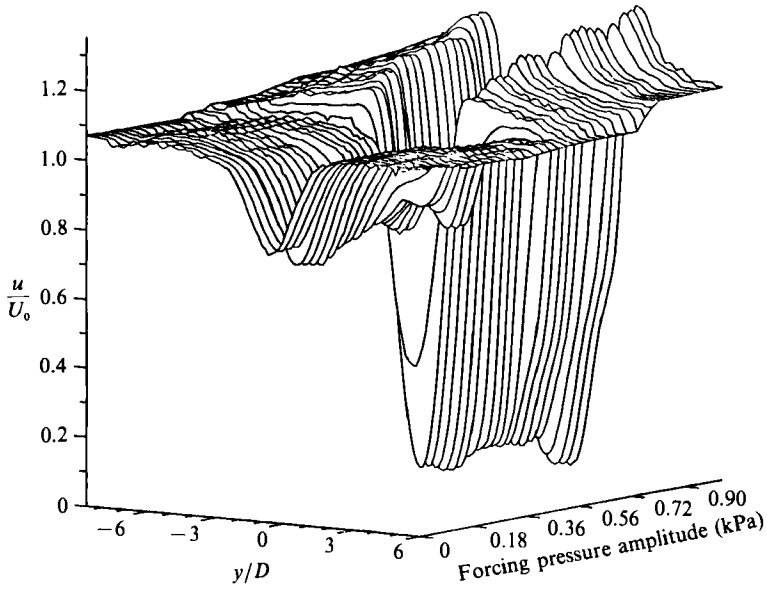

FIGURE 6. Mean velocity profiles plotted against forcing amplitude to show threshold behaviour with $f_e/f_0 = 1.9$ at $Re = 370$ and $x/D = 5$.

Increasing the forcing amplitude to the over-forced flow regime causes the velocity profile to become U-shaped. The peak in the u' r.m.s. decreases to about $0.16U_0$ as a result of the breakdown in the resonance mechanism. The centreline velocity goes to zero, indicating that the fluid in the central portion of the wake is motionless. No significant recirculation of fluid is found in this region. In fact, hydrogen bubbles tend to float straight upward. From flow visualization studies, it appears that the two shear layers develop independently for about 6 diameters downstream of the cylinder. At this point they begin to interact and a new sinuous type of instability develops.

A set of mean velocity profiles obtained by Amato (1989) at $x/D = 5$ and Reynolds number 370 have been superposed in figure 6 to illustrate the threshold character of the over-forced flow regime. Starting with the unforced wake, the V-shaped mean velocity profiles gradually evolve into a W-shaped profile as the forcing amplitude is increased. Above the threshold excitation level, C_b^*, there is a sudden change to the U-shaped profile. No further changes occur when the forcing amplitude is increased. The threshold type of behaviour is unique to the symmetric forcing. When antisymmetric disturbances are used the centreline velocity defect increases, but the sudden change to a U-shaped profile is not seen.

The three regimes of mean profile structure are sensitive to both the forcing frequency and amplitude. A map of the mean velocity profile shapes as a function of forcing frequency and amplitude is shown in figure 7 for symmetric forcing. The envelope of the forcing conditions that could be achieved in this experiment has been outlined by the thick solid line. The shading indicates the region between $1.0 < f_e/f_0 < 2.0$ where W-shaped profiles are found. The top of the shaded region corresponds to C_b^*. The value of C_b^* decreases monotonically as the forcing frequency increases. The W-shaped profiles did not form, when $f_e/f_0 > 2$. At the high forcing frequencies, the mean profiles change directly from a V-shape to a U-shape as the forcing amplitude exceeds C_b^*.

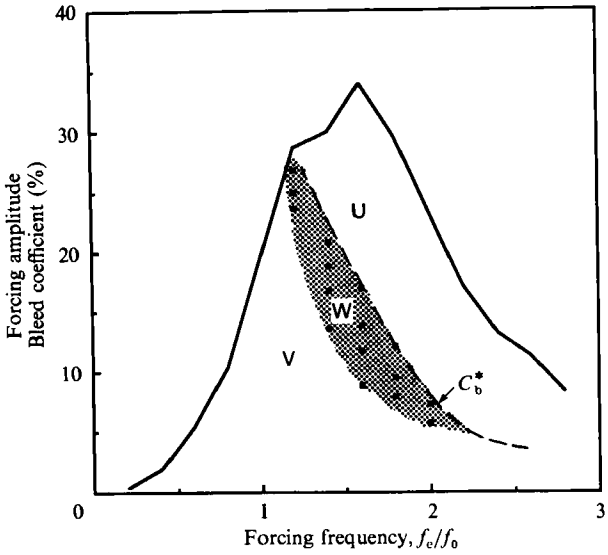

FIGURE 7. Parameter map of the mean flow showing regions of V-, W- and U-shaped velocity profiles at $x/D = 4.0$.

3.2. *Symmetric forcing – unsteady flow behaviour*

The effects of different forcing frequencies on the wake structure are best viewed through the spectra, amplitude and phase distributions of the various modes. All the data presented in this section were obtained at $x/D = 4.0$ and $Re = 470$. For comparison, the spectra of the natural wake are presented in figure 8(*a*) for y-locations corresponding to the peak in the r.m.s. ($y/D = 1.0$) and figure 8(*b*) on the wake centreline ($y/D = 0$). The vortex shedding frequency, f_0, is the strongest peak in the shear-layer spectrum at $f_0 = 1.07$ Hz. A smaller peak corresponding to the first harmonic $f_1 = 2.14$ Hz appears in the centreline spectrum. These were the only significant peaks found in the natural wake spectrum.

Marasli, Champagne & Wygnanski (1989) recognized that the disturbances in the wake could be decomposed into even and odd function of y representing the varicose and sinuous modes. We have used this technique to get a better description of the wake structure by computing the ratio of the energy in the even (varicose) and odd (sinuous) components of each mode. In Marasli *et al.*'s technique the real and imaginary components of the eigenfunction at a particular frequency are decomposed into even and odd functions of y about the wake centreline. The real and imaginary components of the odd functions are then recombined to form the amplitude, $u_{\text{odd}}(y)$, and phase distributions for the odd mode. The same process is repeated for the even functions, to get the amplitude, $u_{\text{even}}(y)$, and phase distributions for the even mode. We carry the technique one step further by computing the energy of the odd and even functions from the square of the amplitude distribution, and integrating across the wake. Two integral quantities have been defined,

$$O = \int_{-h}^{h} u_{\text{odd}}(y)^2 \, \mathrm{d}y, \quad E = \int_{-h}^{h} u_{\text{even}}(y)^2 \, \mathrm{d}y,$$

where $\pm h$ are the limits to the scan in the y-direction. The relative energy in the antisymmetric component of the mode compared to the energy in the symmetric component is expressed by the ratio O/E. When $O/E > 1$ the sinuous (antisymmetric)

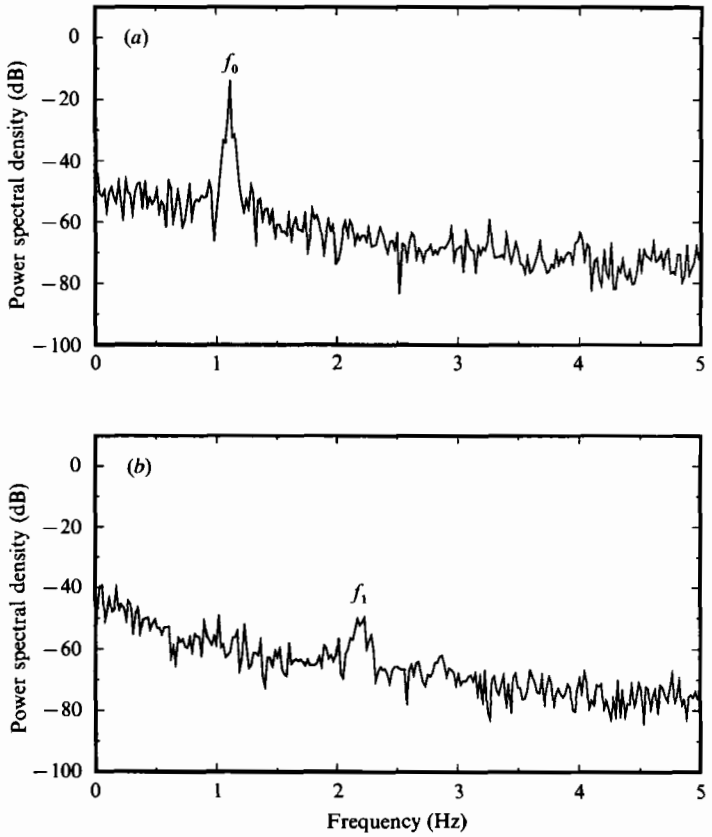

FIGURE 8. Natural wake spectra at $x/D = 4.0$: (*a*) $y/D = 1.0$, peak in r.m.s.; (*b*) centreline, $y/D = 0$.

component of the mode is dominant, and when $O/E < 1$ the varicose (symmetric) component is dominant.

An example of the modal decomposition of the fundamental and its harmonic is shown in figure 9(*a*, *b*) for the natural wake. In these figures the solid line is the combined mode shape obtained from the spectral analysis. the long-dashed line shows the odd component of the mode, and the short-dashed line is the even component. In figure 9(*a*) the vortex shedding mode $f_0 = 1.07$ Hz has $O/E = 4.9$, so it is antisymmetric. One can easily see in the figure that the majority of the energy at this frequency is contained in the antisymmetric mode. The first harmonic at $f_1 = 2.14$ Hz shown in figure 9(*b*) is symmetric, because $O/E = 0.23$. These results support Morkovin's (1987) observation that the symmetry of the disturbance field in an idealized (parallel and infinite) Kármán vortex street is equivalent to the superposition of a sinuous (odd) velocity mode with a varicose (even) velocity mode at twice the vortex shedding frequency.

When low-amplitude symmetric disturbances are introduced into the boundary layer on the cylinder, there is a progressive shift of the shedding frequency toward lower values. The notation used for the shifted vortex shedding frequency is $f_{0'}$. The amount of the frequency shift depends on the forcing amplitude and frequency, which is an effect seen in the global forcing results of Detemple-Laake & Eckelmann (1989) and Barbi *et al.* (1986). Nonlinear interaction between the forcing signal, f_e, and the shifted oscillation frequency, $f_{0'}$, generates sum and difference frequencies in

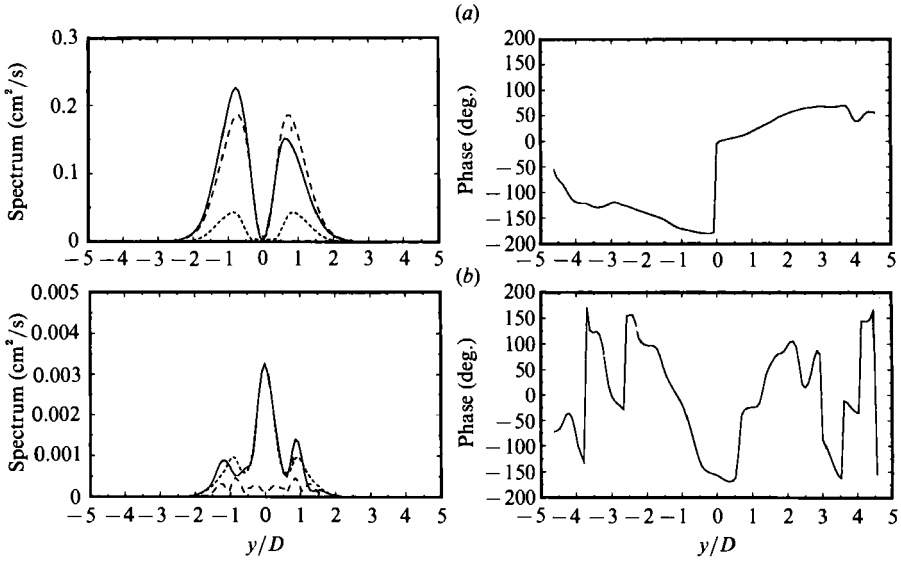

FIGURE 9. Amplitude and phase distributions for modes (*a*) $f_0 = 1.07$ Hz, $O/E = 4.9$; and (*b*) $f_1 = 2.14$ Hz, $O/E = 0.23$, in the unforced wake; ——, the non-decomposed distribution; – – –, the odd component; ----, the even component.

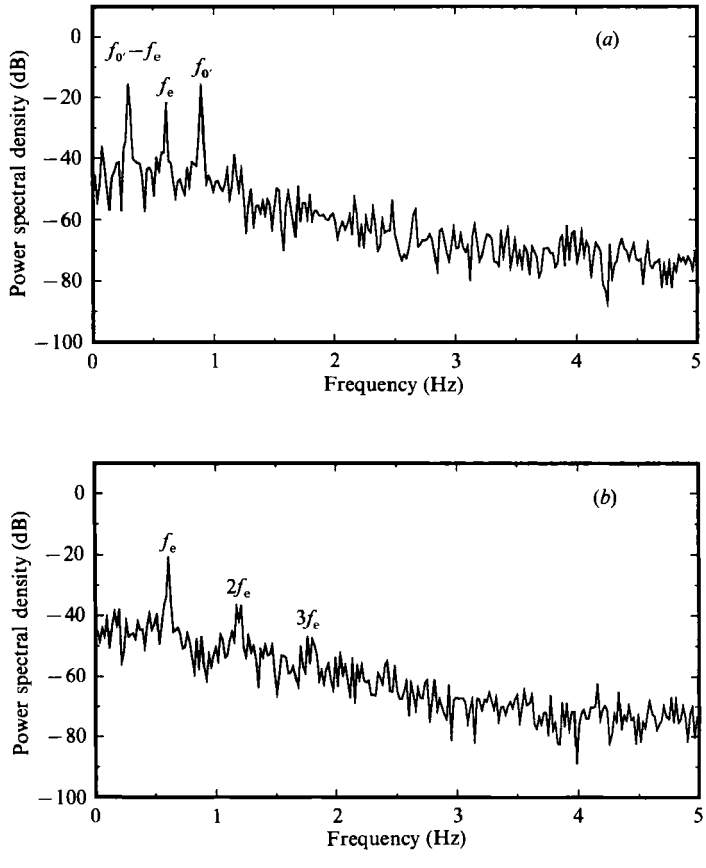

FIGURE 10. Spectra at $x/D = 4.0$ with forcing at 0.6 Hz, $C_b = 0.049$: (*a*) $y/D = 0.6$, (*b*) $y/D = 0$.

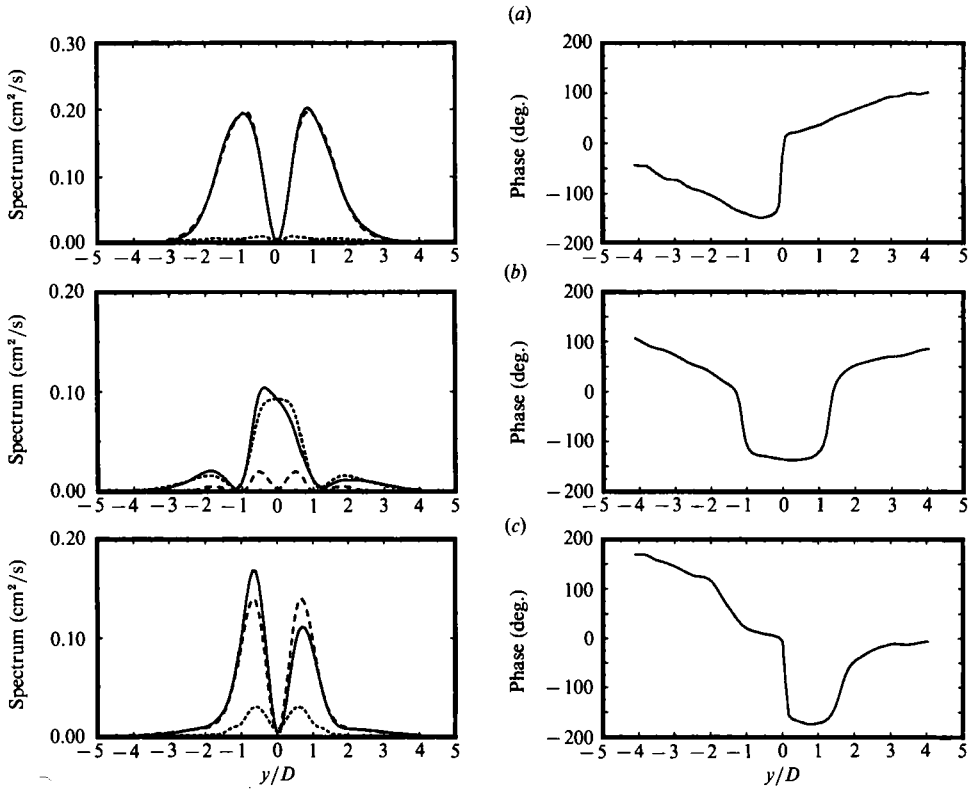

FIGURE 11. Amplitude and phase distributions of the spectral peaks in figure 10(*a*); (*a*) $f_{0'} = 0.9$ Hz, $O/E = 15.0$; (*b*) $f_e = 0.6$ Hz, $O/E = 0.19$, (*c*) $f_{0'} - f_e = 0.3$ Hz, $O/E = 4.6$. ——, The non-decomposed distribution; --- the odd component; ----, the even component.

the spectrum. The spectrum located at a maximum in the u' r.m.s. distribution is presented in figure 10(*a*) corresponding to forcing at $f_e = 0.6$ Hz, $C_b = 0.049$. The dominant spectral peaks are found at $f_e = 0.6$ Hz, $f_{0'} = 0.9$ Hz, and $f_{0'} - f_e = \frac{1}{2}f_e = 0.3$ Hz. The presence of the difference mode indicates that a beating signal has been created between the forced oscillations and the shifted vortex shedding oscillation. The results show that even at the lowest forcing amplitude, the disturbances can grow to a sufficient amplitude for nonlinear interaction to occur.

A comparison of the amplitude of the $f_{0'}$ peak in figure 10(*a*) to the f_0 peak in the spectrum of the unforced wake in figure 8(*a*) indicates that the energy in $f_{0'}$ has decreased approximately 5 dB from the energy in f_0. The symmetric forcing has redistributed the energy into the $\frac{1}{2}f_e$ peak at the expense of $f_{0'}$. The spectrum in figure 10(*b*) was computed from the signal on the wake centreline. Peaks are located at $f_e = 0.6$ Hz, $2f_e = 1.2$ Hz and $3f_e = 1.8$ Hz, and all are even functions with O/E ratios of 0.19, 0.16 and 0.23, respectively. The $f_{0'}$ mode is plotted in figure 11(*a*), where it is seen that symmetric forcing has increased the amount of antisymmetry to $O/E = 15.0$. The amplitude and phase distribution of the f_e mode in figure 11(*b*) shows that it is an even mode with $O/E = 0.19$. The interaction between $f_{0'}$ and f_e creates another sinuous mode at $\frac{1}{2}f_e = 0.3$ Hz with $O/E = 4.6$. The sinuous nature of $f_{0'}$ is evident by the characteristic 180° phase shift and local velocity minimum on the wake centreline. The uniform phase distribution across the centreline for the f_e mode is an indication of the varicose behaviour as seen in figure 11(*b*).

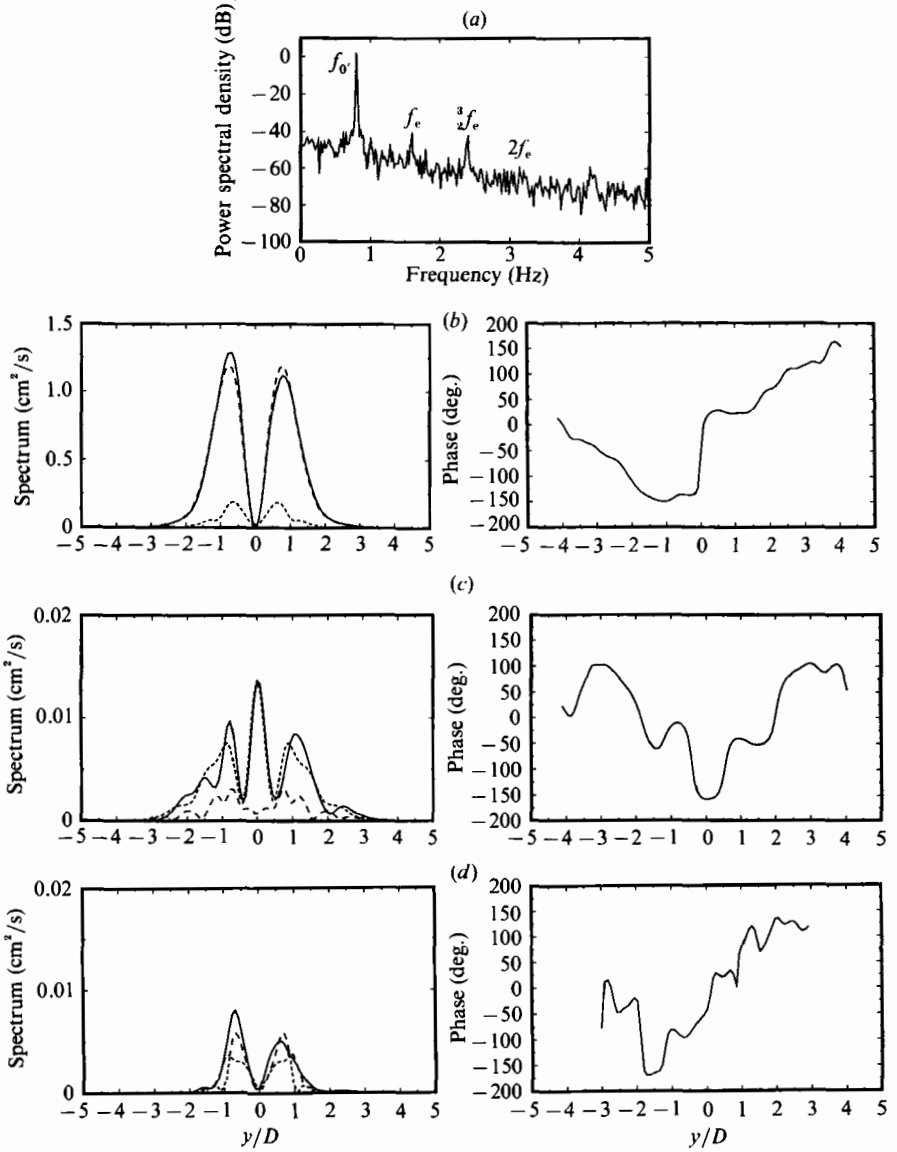

FIGURE 12. Spectra, amplitude and phase distributions for $f_e = 1.6$ Hz, $C_b = 0.14$, $x/D = 4.0$: (*a*) spectrum at r.m.s. peak, $y/D = 0.77$; (*b*) amplitude and phase for $f_{0'} = 0.8$ Hz, $O/E = 7.8$; (*c*) amplitude and phase for $f_e = 1.6$ Hz, $O/E = 0.29$; (*d*) amplitude and phase for $\frac{3}{2}f_e = 2.4$ Hz, $O/E = 1.6$. ——, the non-decomposed distribution; – – – the odd component; ----, the even component.

The symmetry of the combination modes follows two fundamental rules in all of the cases examined in this experiment. First, when nonlinear interactions occur between an even mode and an odd mode, the combination mode will be an odd function of y. Second, if two even modes or two odd modes interact, then the resulting combination mode is even. These could have been anticipated given the quadratic nonlinearity of the governing equations. Therefore, we expect the harmonics resulting from the nonlinear self-interaction of either even or odd modes to be even functions of y. The $\frac{1}{2}f_e$ mode in figure 11 (*c*) is an example of odd–even interaction. The amplitude and phase are shown for the odd mode $f_{0'} - f_e = \frac{1}{2}f_e =$

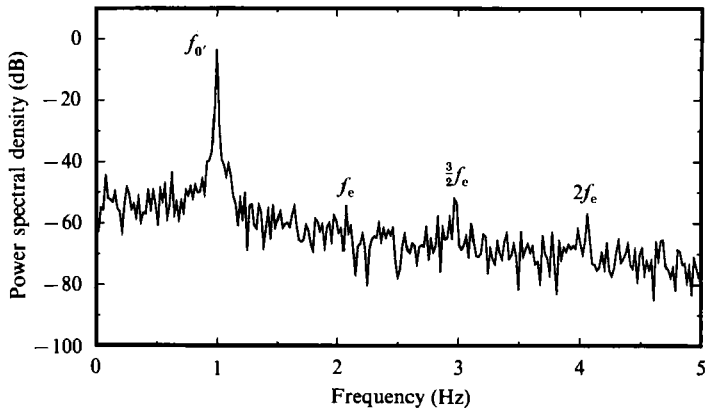

FIGURE 13. Spectrum at $y/D = 1.0$ for forcing at $f_e = 2.0$ Hz, $C_b = 0.072$. Symmetric forcing at this frequency reinforces the natural wake oscillation mode.

0.3 Hz that results from the interaction of the even forcing mode f_e and the odd vortex shedding mode $f_{0'}$. In this case $O/E = 4.6$.

The intermediate level of symmetric forcing amplitude is characterized by the dominance of a sinuous mode at half the forcing frequency, $\frac{1}{2}f_e$, and the complete suppression of the original vortex shedding mode. When $1 < f_e/f_0 < 2$, then W-shaped mean profiles are formed. The data in figure 12 (*a–d*) shows an example of the wake response to symmetric forcing at $f_e = 1.6$ Hz, $C_b = 0.14$. The spectrum in figure 12 (*a*) shows that the vortex shedding at $f_{0'} = \frac{1}{2}f_e = 0.8$ Hz is 40 dB stronger than the forcing peak. (We use the same notation $f_{0'}$ to refer to the new shedding frequency, even though it is a new peak, not a progressively shifted frequency.) Obviously, there is very strong coupling between the symmetric forcing f_e and the antisymmetric mode $\frac{1}{2}f_e$. The vortex shedding mode is sinuous ($O/E = 7.8$) with the 180° phase shift occurring on the wake centreline as shown by the phase plot in figure 12 (*b*). In figure 12 (*c*) the harmonic mode $f_1 = f_e$ (same frequency as the forcing frequency) is symmetric with $O/E = 0.29$. Both flow visualization and measurements of the phase of the shedding frequency along the axis of the cylinder indicate the vortex shedding is parallel to the axis of the cylinder, so the dominant modes are two-dimensional.

The amplitude and phase distributions are shown in figure 12 (*d*) for a weak mode at $\frac{3}{2}f_e = 2.4$ Hz, which results from the interaction of the even forcing field and the odd fundamental mode. Following the earlier arguments we expect the 2.4 Hz mode to be an odd function of y, which is verified by $O/E = 1.6$. A fourth peak at $2f_e = 3.2$ Hz can also be seen in the spectrum in figure 12 (*a*). This peak results from either the self-interaction of f_e (an even mode) or through the interaction of $\frac{1}{2}f_e$ (odd) with $\frac{3}{2}f_e$ (odd mode). An even mode is expected in either case, and indeed $2f_e$ is even with $O/E = 0.62$.

The spectrum in figure 12 (*a*) demonstrates that symmetric forcing suppresses the natural oscillations in favour of vortex shedding at $\frac{1}{2}f_e$. It appears that the symmetric forcing channels energy into an antisymmetric mode at half the forcing frequency. Since the natural vortex shedding frequency was 1.0 Hz, one would expect forcing at 2.0 Hz to reinforce the Kármán shedding. Indeed this is verified by the spectrum shown in figure 13 for excitation at $f_e = 2.0$ Hz, $C_b = 0.072$, at $y/D = 1.0$. The amplitude of the 1.0 Hz spectral peak increases from −15 dB in the unforced case to −5 dB. In contrast to the natural wake spectrum in figure 8 (*a*), the spectrum in figure 13 shows four peaks, at $\frac{1}{2}f_e$, f_e (very weak), $\frac{3}{2}f_e$ and $2f_e$, which are at the same

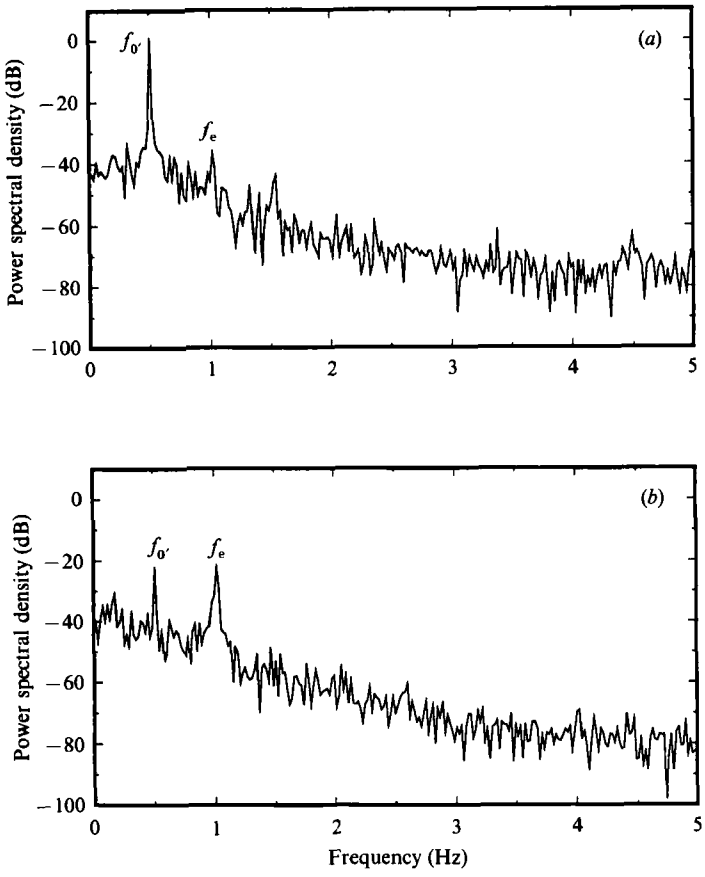

FIGURE 14. Spectra for symmetric forcing at $f_e = 1.0$ Hz, $C_b = 0.14$, $x/D = 4.0$: (*a*) spectrum at r.m.s. peak, $y/D = 0.94$; (*b*) $y/D = 0$.

frequency ratios (f/f_e) as in the 1.6 Hz forced case. However, the distribution of energy among the peaks is different. Although the forcing amplitude is only half the value of the previous case, i.e. $C_b = 0.072$ compared to $C_b = 0.14$ for $f_e = 1.6$, the amplitude of the fundamental peak is close to the same value of -3 dB. It is not surprising that the energy transfer to the fundamental is more efficient when the fundamental sinuous mode is close to the natural shedding frequency, since it is the preferred mode.

Next we examined if symmetric forcing at $f_e = f_0 = 1.0$ Hz would reinforce the antisymmetric f_0 mode, or if the energy would continue to be transferred to the $\frac{1}{2}f_e$ mode as observed in the previous cases. The spectra at $y/D = 0.94$ and 0 in figure 14(*a*, *b*) confirm that forcing at $C_b = 0.14$ exhibits the same behaviour as the other intermediate forcing cases. A new vortex shedding frequency appears at $f_{0'} = \frac{1}{2}f_e = 0.5$ Hz with $O/E = 3.8$, instead of reinforcing the antisymmetric f_0 mode. The amplitude and phase for $f_{0'}$ have been plotted in figure 15(*a*). The original antisymmetric vortex shedding mode was replaced by the symmetric mode at $f_e = 1.0$ Hz, $O/E = 0.32$ shown in figure 15(*b*). These results suggest that the symmetric first harmonic of the vortex shedding mode is an important element for controlling the energy transfer in the wake. The true test comes from comparison with antisymmetric forcing experiments.

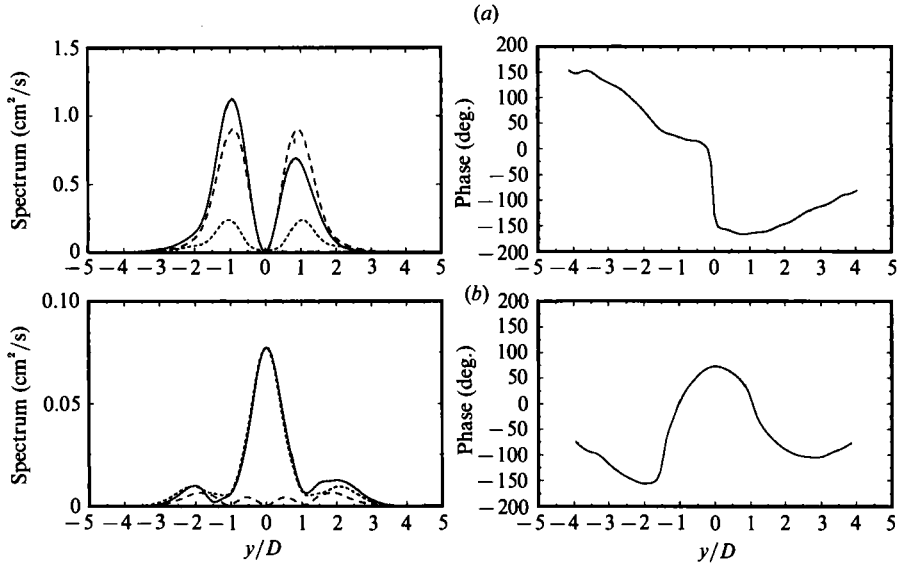

FIGURE 15. Amplitude and phase distributions for $f_e = 1.0$ Hz, $C_b = 0.14$: (*a*) $f_{0'} = 0.5$ Hz, $O/E = 3.8$; (*b*) $f_e = 1.0$ Hz, $O/E = 0.32$: ——, the non-decomposed distribution; – – –, the odd component; ---- the even component.

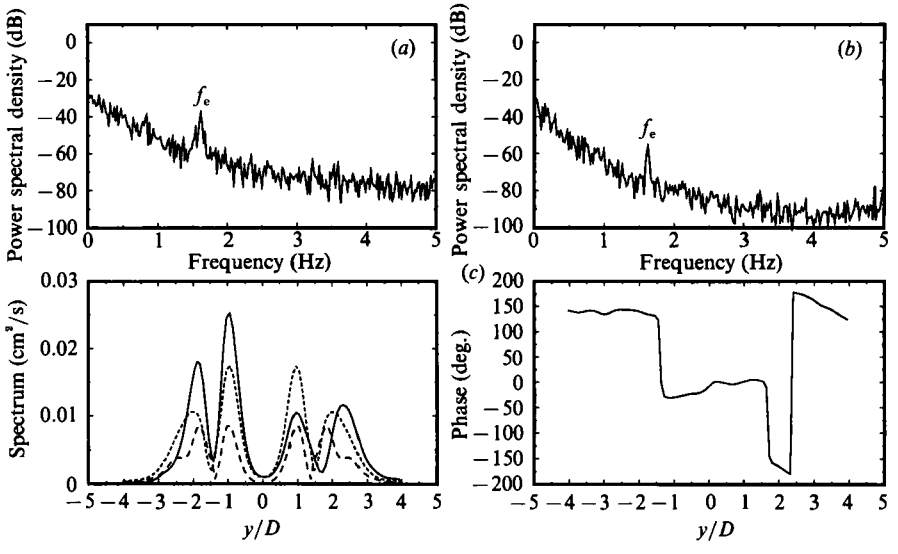

FIGURE 16. Spectra in the over-forced flow state, $f_e = 1.6$ Hz, $C_b = 0.34$: (*a*) $y/D = 1.6$; (*b*) $y/D = 0$. (*c*) Amplitude and phase for $f_e = 1.6$ Hz, $O/E = 0.59$: ——, the non-decomposed distribution; – – –, the odd component; ----, the even component.

The over-forced regime is entered when the forcing amplitude exceeds the threshold level, C_b^* shown in figure 7. It is apparent from the flow visualization in figure 4(*d*) that the large-scale Kármán vortices no longer form in the near-wake region, although a weak sinuous motion of the wake appears farther downstream. Figure 16(*a*, *b*) shows the spectra obtained at y-locations corresponding to the peak in the r.m.s. distribution at $y/D = 1.6$ and on the centreline of the wake for

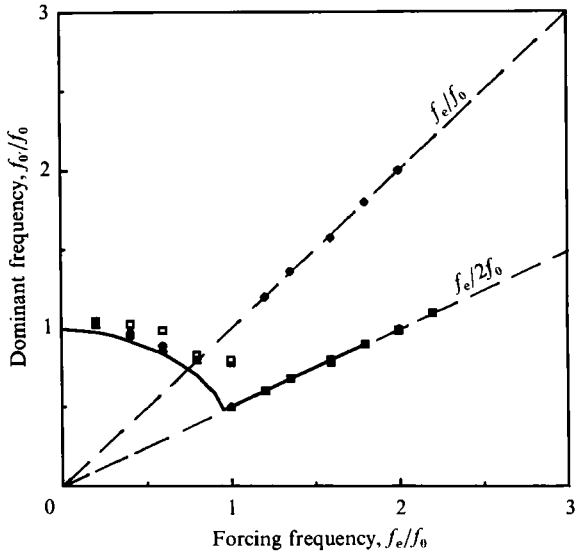

FIGURE 17. Dominant wake response frequency dependence on the forcing frequency with symmetric excitation: □, low amplitude; △, medium amplitude; ◇, high amplitude; ——, the results of Barbi *et al.* (1986); ---, $f_{0'}/f_0 = f_e/f_0$ and $f_{0'}/f_0 = f_e/2f_0$ lines.

symmetric forcing at $f_e = 1.6$ Hz and $C_b = 0.34$. The forcing frequency appears as the strongest peak in figure 16(*a*). From figure 16(*c*) one sees that the excitation mode, f_e, remains an even function with $O/E = 0.6$.

The important observation is that increasing the forcing amplitude from $C_b = 0.14$ in figure 12 to $C_b = 0.34$ in figure 16 causes the peak in the fundamental to drop from 0 to -30 dB. Clearly the mechanism for self-excitation has been disrupted. Furthermore, the decrease in the energy of oscillation is evidence that the energy in the vortex shedding mode does not come solely from the forcing field. Without the resonance mechanism the fluctuation energy levels are much lower, even though the forcing amplitudes are higher. We believe that the two shear layers in the over-forced case are developing independently, i.e. the cross-flow interaction has apparently ceased. Analogous to the splitter plate experiments, the large-scale Kármán vortices do not form.

The frequency response of the wake to the symmetric excitation is summarized in figure 17. The dominant frequency appearing in the wake has been plotted against the forcing frequency, where both have been normalized by the natural shedding frequency, f_0. The progressive shift of $f_{0'}$ to frequencies slightly lower than the natural f_0 occurs at low-amplitude forcing levels and frequencies f_e/f_0 between 0 and 1.5. Medium-amplitude forcing causes the data to fall on the $\frac{1}{2}f_e$ line when the forcing f_e/f_0 is greater than 1.0. Forcing levels above C_b^* place the dominant frequencies on the f_e/f_0 line.

There is striking similarity between the low-Reynolds-number results in figure 17 and the results of an experiment by Barbi *et al.* (1986) at high Reynolds number, superposed as the solid line. In Barbi's experiment, which was conducted at Reynolds number 40000, the flow was forced by oscillating the free-stream velocity. The purpose of their experiment was to compare these results to the oscillating cylinder experiments. In both types of excitation the boundary layers on the body of the cylinder are modulated in phase, analogous to the local symmetric forcing used

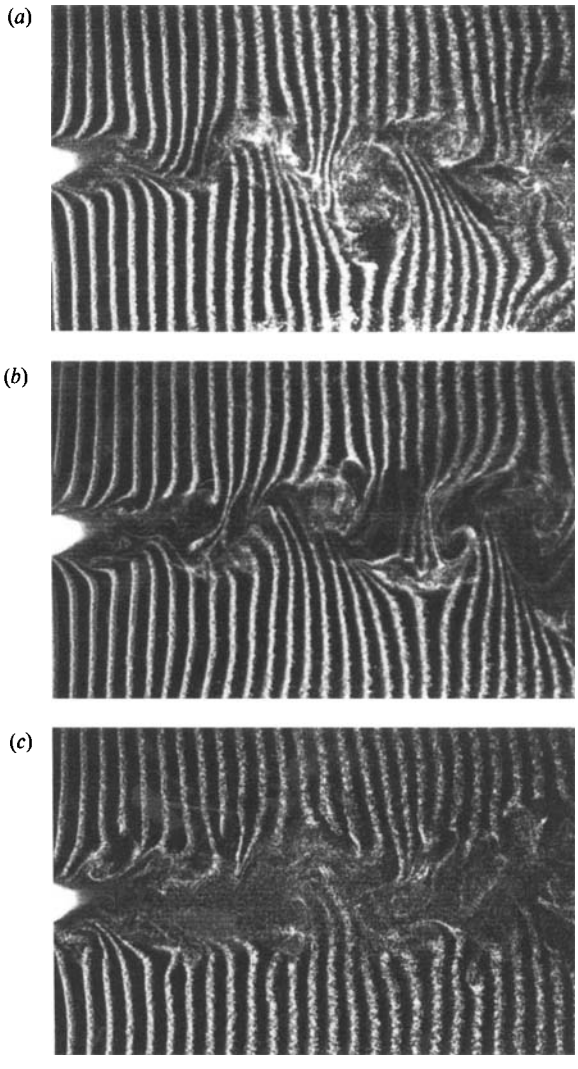

FIGURE 18. Flow visualization for antisymmetric forcing $f_e/f_0 = 2.0$: (*a*) $C_b = 0.004$; (*b*) $C_b = 0.019$; (*c*) $C_b = 0.073$.

in the present experiment. The close agreement between Barbi's results and the results of this experiment provides strong evidence that global types of forcing change the wake structure by modulating the boundary layer. Modulation of the boundary layer modifies the vorticity production on the surface, hence the distribution of vorticity and the vortex development are also affected. This implies that the significant region of interaction occurs on the surface of the cylinder when global types of forcing are used to modify the wake structure.

3.3. *Antisymmetric forcing*

It is necessary to excite the boundary layers with *antisymmetric* disturbances to confirm that the results described in the previous sections are truly dependent on the symmetry of the forcing field. The antisymmetric excitation was produced by forcing the two rows of holes 180° out of phase. Flow visualization photographs are shown

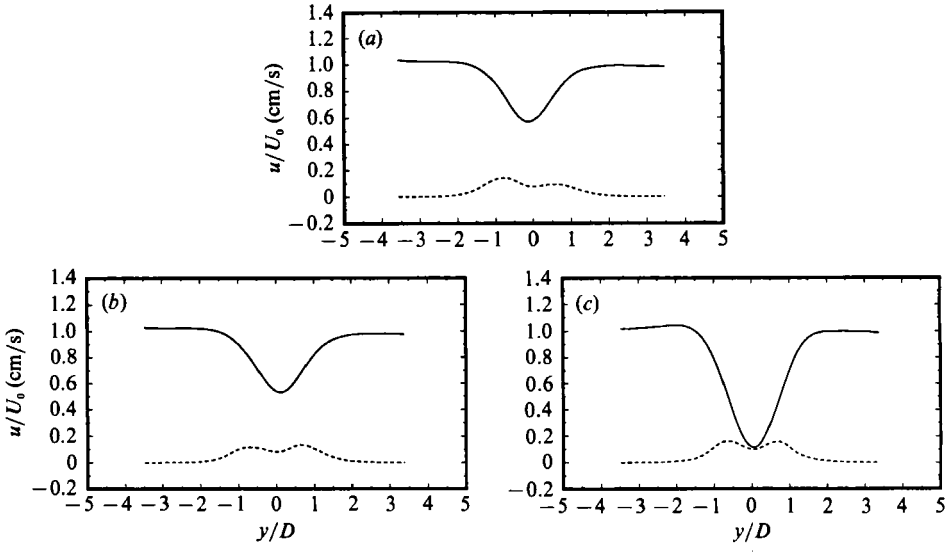

FIGURE 19. Mean and r.m.s. velocity profiles for antisymmetric forcing $f_e = 2.0$ Hz: (a) $C_b = 0.004$; (b) $C_b = 0.019$, (c) $C_b = 0.073$. ——, The mean profile; ----, the r.m.s. profile.

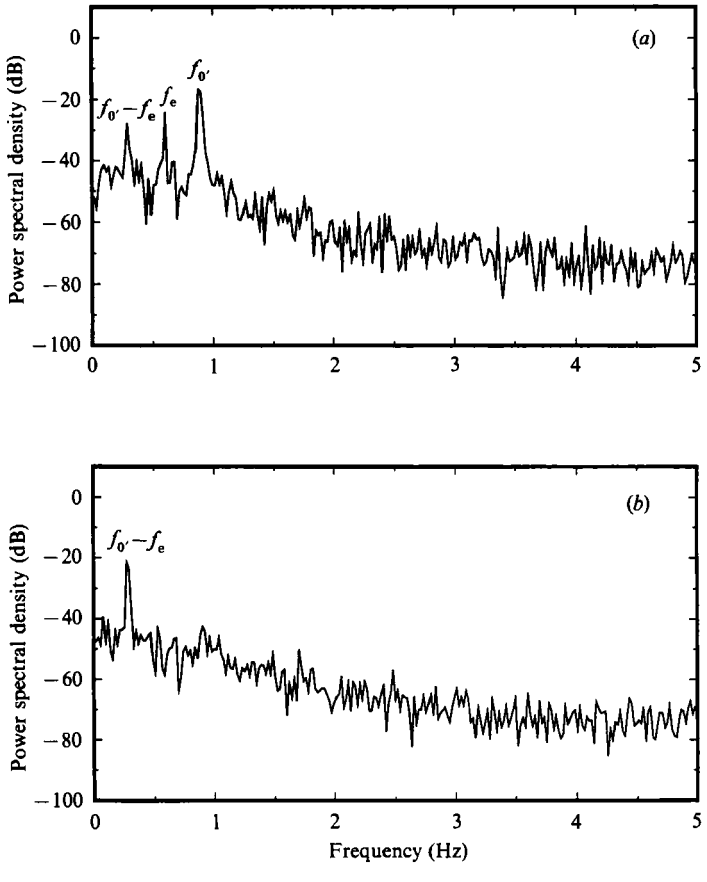

FIGURE 20. Spectra of antisymmetric forcing at $f_e = 0.61$ Hz, $C_b = 0.056$: (a) $y/D = 0.63$; (b) $y/D = 0$.

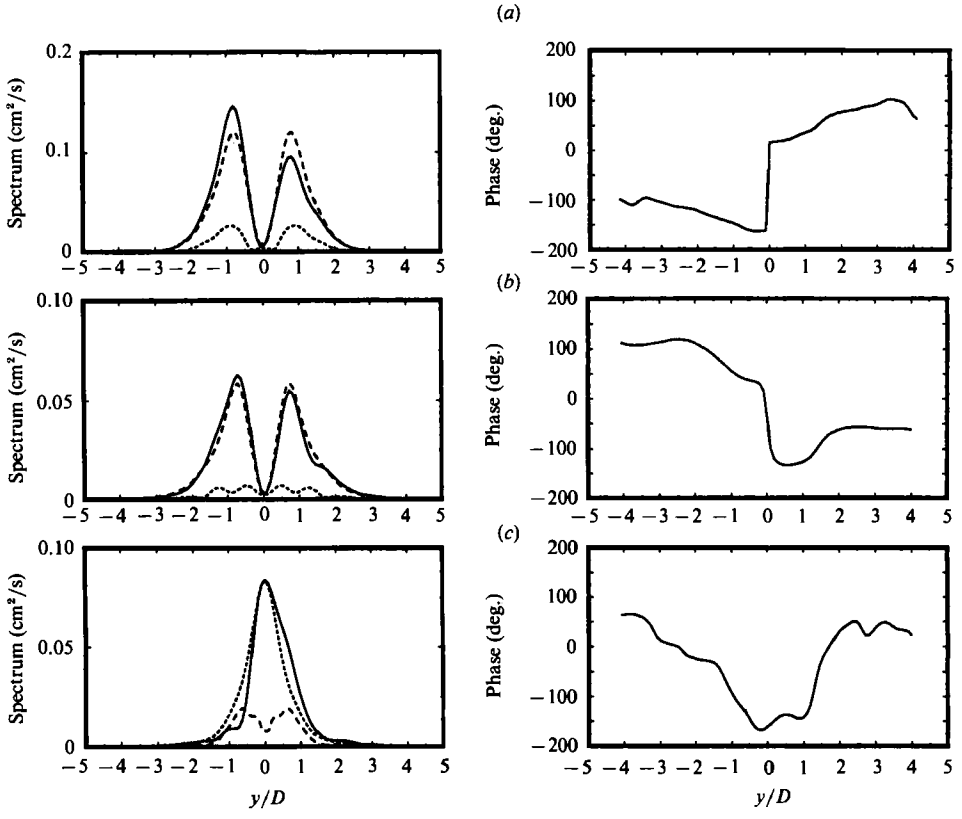

FIGURE 21. Amplitude and phase distributions for antisymmetric forcing: (*a*) $f_{0'} = 0.92$ Hz, $O/E = 4.6$; (*b*) $f_e = 0.61$ Hz, $O/E = 7.0$; (*c*) $f_{0'} - f_e = 0.29$ Hz, $O/E = 0.33$. ——, The non-decomposed distribution; – – –, the odd component; ----, the even component.

in figure 18(*a*–*c*) corresponding to $f_e = 2.0$ Hz and $C_b = 0.004$, 0.019 and 0.073, respectively. It is evident that the wake does not respond to the antisymmetric forcing with the rich variation in structure found with symmetric forcing. Even at the largest forcing amplitudes, the wake does not appear to form the sea-horse pattern of vortices. In all cases the dominant mode appears to be sinuous.

Mean and r.m.s. velocity profiles at $x/D = 4.0$ for antisymmetric forcing are shown in figure 19(*a*–*c*), corresponding to the same conditions as the flow visualization. The mean profile is V-shaped in all cases, with a centreline defect that increases with increasing forcing amplitude. As predicted from the flow visualization, no W-shaped velocity profile region was found. No threshold behaviour was observed, although the velocity defect became quite large. These results confirm that the wake structure is sensitive to the symmetry of the forcing field.

Spectra show that the majority of the forcing energy remains in the vortex shedding mode $f_{0'}$ at low and intermediate forcing amplitudes. Combination modes are formed by interaction between the vortex shedding and forcing frequencies. At high forcing amplitudes, the vortex shedding locks-on to the forcing frequency.

An example of the unsteady flow behaviour under antisymmetric forcing conditions is shown by the spectra at $y/D = 0.63$ and 0 in figure 20(*a*, *b*) respectively, for forcing at 0.61 Hz and $C_b = 0.056$. Note that to obtain a similar effect in the symmetric forcing case of §3.2, C_b was 0.049. One finds three significant peaks in the

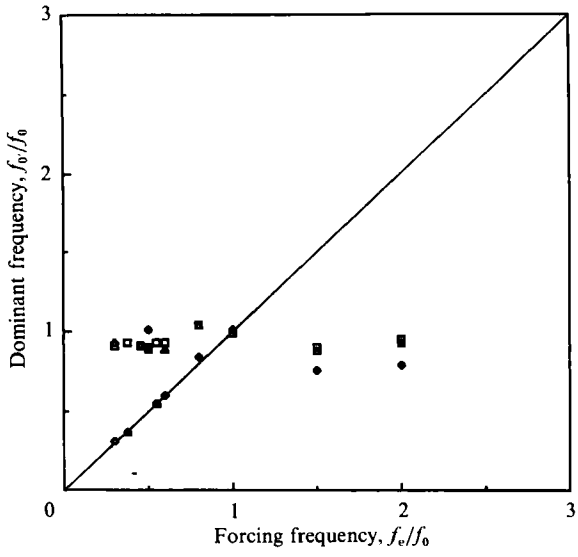

FIGURE 22. Dominant wake response frequency dependence on the forcing frequency with antisymmetric excitation: □, low amplitude; △, medium amplitude; ◇, high amplitude; ——, $f_{0'}/f_0 = f_e/f_0$.

spectrum at $y/D = 0.63$: at $f_{0'} = 0.92$ Hz, $f_e = 0.61$ Hz and $f_0 - f_e = 0.29$ Hz. The amplitude and phase distributions for the three modes are shown in figure 21 (*a–c*) for the $f_{0'}/f_e$ and $f_{0'} - f_e$ modes, respectively. As predicted by the 'symmetry rules' the difference mode is now an *even* function ($O/E = 0.33$), because the interacting modes are both odd functions, i.e. $O/E = 4.6$ for the $f_{0'}$ mode and $O/E = 7.0$ for the f_e mode. This result supports the earlier hypothesis that the symmetry of the forcing field is a controlling element in the vortex formation process. Clearly, there must be a fundamental difference in the wake structure between symmetric and antisymmetric forcing, because the symmetry of the combination modes depends on the symmetry of the forcing mode.

The dependence of the dominant frequency on the antisymmetric forcing frequency is summarized in figure 22. At low forcing levels the dominant mode is close to the natural shedding frequency and independent of f_e. As the forcing level is increased there is a progressive shift of the shedding frequency by a few percent to lower values. Beating occurs at the difference frequency between the forcing field and the natural wake oscillation frequency in the low- ($C_b = 0.017$) and intermediate- ($C_b = 0.052$) amplitude range. At high forcing amplitudes, $C_b > 0.08$, the forcing frequency becomes dominant when $f_e/f_0 < 1.0$. However, in contrast to the symmetric forcing cases, the natural wake oscillation was never completely suppressed.

4. Discussion

In any experiment at supercritical Reynolds numbers the wake is in a self-excited state. A type-I or type-II global instability provides feedback from the unsteady vortices in the wake to the body, which establishes the initial disturbance field. When local forcing is applied different regimes of behaviour occur, depending on the symmetry and relative amplitude between the forcing field and the initial disturbance

field. For both symmetric and antisymmetric forcing at low levels, the dominant frequency is determined by the natural wake oscillation mechanism. Even when the forcing field is at very low levels, the disturbances can amplify to a strength that allows nonlinear interaction to occur with the original wake oscillation. This produces a beating signal at the absolute value of the difference frequency $|f_{0'}-f_e|$, which can be quite strong. The symmetry of the difference mode is determined by the symmetry of the forcing field. By the symmetry rule the antisymmetric forcing produces a symmetric difference mode, while an antisymmetric difference mode is formed by a symmetric forcing field. Therefore, the wake structure depends on the symmetry of the forcing field.

The near-wake oscillation mechanism has been found to be surprisingly sensitive to symmetric disturbances over a range of forcing frequencies. Morkovin (1987) has speculated that the wake would be receptive to symmetric oscillations at twice the Kármán shedding frequency. Clearly this is true, but it goes beyond the sensitivity at just one frequency. The results have shown that the shedding frequency can be controlled by the symmetric disturbance frequency. Raising the forcing amplitude to intermediate levels creates a different spectrum with symmetric forcing than with antisymmetric forcing. In the symmetric case the forcing frequency determines the wake oscillation frequency, which appears at the subharmonic of the forcing frequency, $\frac{1}{2}f_e$. The natural wake oscillations are completely suppressed at intermediate forcing levels.

The forcing field dominates the wake spectrum when high-amplitude forcing levels are used. For symmetric forcing above C_b^*, the results have shown that the antisymmetric mode which generates the large-scale Kármán vortex street is disrupted, and the staggered vortex pattern breaks down into a parallel arrangement of vortices. the near wake no longer supports the growth of the antisymmetric component. The energy of the symmetric oscillations at f_e is much weaker in the over-forced state, and flow visualization shows that the vortices are much smaller in size. At high amplitudes, antisymmetric forcing causes the wake oscillations to lock-on to the forcing frequency. The sudden change to a U-shaped mean velocity profile was not observed when antisymmetric forcing was applied.

There are two likely explanations for the loss of the resonance in the overforced-flow. First, since the forcing amplitudes are large enough in this experiment for nonlinear effects to occur on the surface of the cylinder, the base flow may have been altered (by second-order effects) to a state that will not amplify the antisymmetric disturbance mode. If the base flow becomes stable to the antisymmetric mode, then only the symmetric mode from the forcing signal will appear in the wake.

Another possible explanation for the behaviour in the over-forced state can be found in concepts of linear theory, keeping in mind the caveat that this flow is strongly nonlinear. Monkewitz & Nguyen (1987) studied the instability characteristics of a family of mean wake profiles, and discovered that the varicose mode of instability is *not* absolutely unstable for typical wake velocity profiles. Without the absolute instability, a global instability would not be supported in the near wake. As the symmetric forcing level is increased, the sinuous feedback signal from the wake will eventually be dominated by the varicose forcing signal. The separating shear layers will be dominated by the varicose mode, but without the absolute instability in the near wake, the global instability will not occur and the large-scale Kármán vortices will not form. Only the disturbances introduced at the surface of the cylinder will be present to convect downstream, which causes the dominant frequency in the wake to appear at the forcing frequency.

It is our opinion that the latter mechanism is the more likely explanation for the breakdown of the resonance, primarily because the mean velocity profiles in the antisymmetric forcing experiments do not show the threshold type of behaviour found with symmetric forcing experiments do not show the threshold type of behaviour found with symmetric forcing. If we assume that the base flow states are independent of the symmetry of the forcing field, then the threshold behaviour seen in the symmetric forcing case must be a result of the unsteady flow effects. however, to conclusively prove that this is the case, a more definitive experiment must be carried out, perhaps using numerical simulation.

5. Conclusion

For the first time in a globally unstable flow it has been shown that the vortex shedding frequency and structure can be changed by introducing local disturbances into the boundary layer on the cylinder. Three general regimes of behaviour were found to depend on the frequency, amplitude and symmetry of the forcing field. At low forcing amplitudes one observes the nonlinear interaction between the modes corresponding to the original wake oscillator and the forced oscillation mode. This leads to combination modes representing a beating between the oscillators. When the symmetric forcing amplitude is increased from low to intermediate forcing levels, the original wake oscillation mode is suppressed in favour of a new vortex shedding mode at half the forcing frequency. Over the frequency range $1 < f_e/f_0 < 2$, a W-shaped mean velocity profile is observed, and the wake appears to spread faster.

An upper limit to the amount of symmetric forcing that can produce an antisymmetric vortex shedding mode has been found. The limit is a frequency-dependent threshold, above which the antisymmetric mode is no longer amplified by the wake. Once this threshold is exceeded the mechanism for large-scale vortex formation ceases, and parallel vortex shedding begins.

Localized forcing with antisymmetric disturbances produces a different wake response than symmetric forcing, which proves the importance of the symmetry of the forcing field. Typical spectra consist of three frequencies, $f_{0'}$, f_e and a beating signal at the absolute value of the difference frequency, $|f_0 - f_e|$. When the forcing amplitude is at the highest levels, the vortex shedding occurs at the forcing frequency.

The cross-flow symmetry of the combination modes resulting from nonlinear interaction could be predicted by two simple rules of symmetry. An odd mode interacting with an even mode always produces an odd mode. Interaction between two odd or two even modes produces an even mode. Such simple rules are helpful in identifying mode interactions and in determining the wake structure.

Many of the features observed in experiments with global forcing, such as the sea-horse pattern of vortices and vortex shedding at half the forcing frequency have been reproduced with the local forcing in the boundary layer. This suggests that the important interaction between the forcing field and the vortex formation mechanism actually occurs on the surface of the cylinder.

The support of the Office of Naval Research under Grant N00014-90-J-1420 monitored by Dr Edwin Rood is gratefully acknowledged.

REFERENCES

AMATO, C. 1989 Unsteady bleed as a flow control technique. M.S. thesis, Mech. & Aero. Eng. Dept. Illinois Institute of Technology.

BARBI, C., FAVIER, D. P., MARESCA, C. A. & TELIONIS, D. P. 1986 Vortex shedding and lock-on of a circular cylinder in oscillatory flow. *J. Fluid Mech.* **170**, 527–544.

BEARMAN, P. W. 1967 The effect of base bleed on the flow behind a two-dimensional model with a blunt trailing edge. *Aero. Q.* **18**, 207–224.

BEARMAN, P. W. 1984 Vortex shedding from oscillating bluff bodies. *Ann. Rev. Fluid Mech.* **16**, 195–222.

BERGER, E. 1976 Suppression of vortex shedding and turbulence behind oscillating cylinders. *Phys. Fluids Suppl.* **10**, 191–193.

BLEVINS, R. D. 1985 The effect of sound on vortex shedding from cylinders. *J. Fluid Mech.* **161**, 217–237.

CHOMAZ, J. M., HUERRE, P. & REDEKOPP, L. G. 1988 Bifurcations to local and global modes in spatially developing flows. *Phys. Rev. Lett.* **60**, 25–28.

DETEMPLE-LAAKE, E. & ECKELMANN, H. 1989 Phenomenology of Kármán vortex streets in oscillatory flow. *Exp. Fluids* **7**, 217–227.

FFOWCS WILLIAMS, J. E. & ZHAO, B. C. 1988 The active control of vortex shedding. In *Intl Symp. on Flow Induced Vibration and Noise*, vol. 1, pp. 51–60. ASME.

GERRARD, J. H. 1978 The wakes of cylindrical bluff bodies at low Reynolds number. *Phil. Trans. R. Soc. Lond.* A **288**, 351–382.

GRIFFIN, O. M. & RAMBERG, S. E. 1976 Vortex shedding from a cylinder vibrating in line with an incident uniform flow. *J. Fluid Mech.* **75**, 257–271.

HANNEMAN, K. & OERETEL, H. 1989 Numerical simulation of the absolutely and convectively unstable wake. *J. Fluid Mech.* **199**, 55–88.

KOCH, W. 1985 Local instability characteristics and frequency determination of self-excited wake flows. *J. Sound Vib.* **99**, 53–83.

KOOPMANN, G. H. 1967 The vortex wakes of vibrating cylinders at low Reynolds numbers. *J. Fluid Mech.* **28**, 501–512.

MARASLI, B., CHAMPAGNE, F. H. & WYGNANSKI, I. 1989 Modal decomposition of velocity signals in a plane, turbulent wake. *J. Fluid Mech.* **198**, 255–273.

MONKEWITZ, P. A. 1988 The absolute and convective nature of instability in two-dimensional wakes at low Reynolds numbers. *Phys. Fluids* **31**, 999–1006.

MONKEWITZ, P. A. & NGUYEN, L. N. 1987 Absolute instability in the near-wake of two-dimensional bluff bodies. *J. Fluids Struc.* **1**, 165–184.

MORKOVIN, M. V. 1964 Flow around circular cylinders – a kaleidoscope of challenging fluid phenomenon. *Symp. on Fully Separated Flows*, pp. 102–118. ASME.

MORKOVIN, M. V. 1987 On symmetry properties of free and forced vortex streets. *Bull. Am. Phys. Soc.* **32**, 2059–2060.

NISHIOKA, M. & SATO, H. 1978 Mechanism of determination of the shedding frequency of vortices behind a cylinder at low Reynolds numbers. *J. Fluid Mech.* **89**, 49–60.

OLINGER, D. J. & SREENIVASAN, K. R. 1988 Nonlinear dynamics of the wake of an oscillating cylinder. *Phys. Rev. Lett.* **60**, 797–800.

PROVENSAL, M., MATHIS, C. & BOYER, L. 1987 Benard–von Kármán instability: transient and forced regimes. *J. Fluid Mech.* **182**, 1–22.

ROCKWELL, D. 1990 Active control of globally unstable separated flow. Invited lecture. *Symp. on Unsteady Flows, Toronto.* ASME.

SREENIVASAN, K. R., STRYKOWSKI, P. J. & OLINGER, D. J. 1987 Hopf bifurcation Landau equation and vortex shedding behind circular cylinders. In *Proc. Forum Unsteady Flow Sep.* (ed. K. N. Ghia), vol. 52, pp. 1–13. ASME.

TRIANTAFYLLOU, G. S., TRIANTAFYLLOU, M. S. & CHRYSSOSTOMIDIS, C. 1986 On the formation of vortex streets behind stationary cylinders, *J. Fluid Mech.* **170**, 461–477.

UNAL, M. F. & ROCKWELL, D. 1987*a* On vortex formation for a cylinder. Part 1. The initial instability. *J. Fluid Mech.* **190**, 491–512.

UNAL, M. F. & ROCKWELL, D. 1987*b* On vortex formation from a cylinder. Part 2. Control by splitter-plate interference. *J. Fluid Mech.* **190**, 513–529.

WEHRMANN, O. H. 1967 Influence of vibrations on the flow field behind a cylinder. *Phys. Fluids Suppl.* **10**, 187–190.

WILLIAMS, D. R. & AMATO, C. 1989 Unsteady pulsing of cylinder wakes. In *Frontiers in Experimental Fluid Mechanics* (ed. M. Gad-el-Hak). Lecture Notes in Engineering, vol. 46, pp. 337–364. Springer.

WILLIAMS, D. R. & ECONOMOU, M. 1987 Scanning laser anemometer measurements of a forced cylinder wake. *Phys. Fluids* **30**, 2283–2285.

WILLIAMSON, C. H. K. & ROSHKO, A. 1988 Vortex formation in the wake of an oscillating cylinder. *J. Fluids Struc.* **2**, 355–381.

WOOD, C. J. 1964 The effect of base bleed on a periodic wake. *J. R. Aeronaut. Soc.* **68**, 477–482.

WOOD, C. J. 1967 Visualization of an incompressible wake with base bleed. *J. Fluid Mech.* **29**, 259–272.